Progress In Electromagnetics Research, PIER 82, 381–400, 2008

TIME DOMAIN INVERSE SCATTERING OF A TWO-DIMENSIONAL HOMOGENOUS DIELECTRIC OBJECT WITH ARBITRARY SHAPE BY PARTICLE SWARM OPTIMIZATION

C.-H. Huang, C.-C. Chiu, C.-L. Li, and K.-C. Chen

Electrical Engineering Department
Tamkang University
Tamsui, Taiwan, R.O.C.

Abstract—This paper presents a computational approach to the two-dimensional time domain inverse scattering problem of a dielectric cylinder based on the finite difference time domain (FDTD) method and the particle swarm optimization (PSO) to determine the shape, location and permittivity of a dielectric cylinder. A pulse is incident upon a homogeneous dielectric cylinder with unknown shape and dielectric constant in free space and the scattered field is recorded outside. By using the scattered field, the shape and permittivity of the dielectric cylinder are reconstructed. The subgridding technique is implemented in the FDTD code for modeling the shape of the cylinder more closely. In order to describe an unknown cylinder with arbitrary shape more effectively, the shape function is expanded by closed cubic-spline function instead of frequently used trigonometric series. The inverse problem is resolved by an optimization approach, and the global searching scheme PSO is then employed to search the parameter space. Numerical results demonstrate that, even when the initial guess is far away from the exact one, good reconstruction can be obtained. In addition, the effects of Gaussian noise on the reconstruction results are investigated. Numerical results show that even the measured scattered E fields are contaminated with some Gaussian noise, PSO can still yield good reconstructed quality.

1. INTRODUCTION

The objective of the inverse scattering is to determine the electromagnetic properties of the scatterer from scattering field measured outside. Inverse scattering problems have attracted much

attention in the past few years. This kind of problem has several important applications such as medical imaging, microwave remote sensing, geophysical exploration, and nondestructive testing.

In the past twenty years, the inversion techniques are developed intensively for the microwave imaging both in frequency domain and time domain [1–25]. Although intrinsic ill-posedness and nonlinearity of these problems appear consequentially in the inverse scattering problems [26–29], the study can be applied in widespread use. Most of the inversion techniques are investigated for the inverse problem using only single frequency scattering data (monochromatic source) [1–11]. However, the time domain scattering data is important for the inverse problem because the available information content about scatterer is more than the only single frequency scattering data. Therefore, various time domain inversion approaches are proposed [12–25] that could be briefly classified as the layer-stripping approach [12], the iterative approach: Born iterative method (BIM) [13–15], the distorted Born iterative method (DBIM) [16], Local Shape Function (LSF) [17] and optimization approach [18–21]. Traditional iterative inverse algorithms are founded on a functional minimization via some gradient-type scheme. In general, during the search of the global minimum, they tend to get trapped in local minima when the initial guess is far from the exact one. Some global optimal searching method such as genetic algorithm [22–24], neural network [25], have be proposed to search the global extreme of the nonlinear functional problem. In the 1995, the Kennnedy and Eberhart first proposed the particle swarm optimization (PSO) [30]. The particle swarm optimization is a population based stochastic optimization algorithm. It is a kind of swarm intelligence that is based on social behavior. In recent year, some researchers have focused on applying PSO in the inverse problem [31–35]. To the best of our knowledge, there is still no investigation on using the PSO to reconstruct the electromagnetic imaging of homogeneous dielectric cylinders with arbitrary shape in free space under time domain.

In this paper, the computational methods combining the FDTD method [36] and the PSO algorithm are presented. The forward problem is solved by the FDTD method, for which the subgridding technique [37] is implemented to closely describe the fine structure of the cylinder. The inverse problem is formulated into an optimization one and then the global searching scheme PSO is used to search the parameter space. Cubic spline Interpolation techniques [38] are employed to reduce the number of parameters needed to closely describe a cylinder of arbitrary shape as compared to the Fourier series expansion. In Section 2, the theoretical formulation for the electromagnetic imaging is presented. The general principle of the PSO

and the way we applied them to the imaging problem are described. Numerical results for various objects of different shapes are given in Section 3. Section 4 is the conclusions.

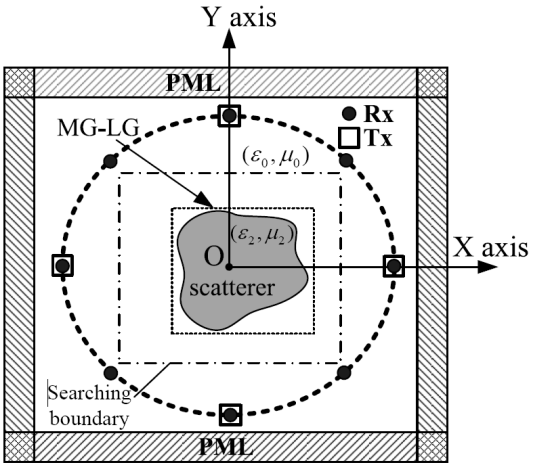

Figure 1. Geometry for the inverse scattering of a arbitrary shape dielectric cylinder in free space.

2. THEORETICAL FORMULATION

Consider a 2-D homogeneous dielectric cylinder in a free space as shown in Figure 1. The cylinder is assumed infinite long in z direction, while the cross-section of the cylinder is arbitrary. The object is illuminated by line source with Gaussian pulse located at these points denoted by Tx around the scatterer. The incident waves of TM_z polarization are generated by a home made FDTD code with fine grid to mimic the experimental data, and only scattered waves are recorded at those points denoted by Rx. The computational domain is discretized by the Yee's cell. It should be mentioned that the computational domain is surrounded by the optimized PML absorber [39] to reduce the reflection from the air-PML interface.

2.1. Forward Problem

The direct scattering problem is to calculate the scattered electric fields while the shape, location and permittivity of the scatterer is given. The shape function $F(\theta)$ of the scatterer is approximated by

the trigonometric series in the direct scattering problem

$$F(\theta) = \sum_{n=0}^{N/2} B_n \cos(n\theta) + \sum_{n=1}^{N/2} C_n \sin(n\theta)$$

In order to closely describe the shape of the cylinder for the forward scattering procedure, the subgridding technique is implemented in the FDTD code, the details are presented as follows.

2.1.1. Subgrid FDTD

A subgridding scheme is employed to divide the problem space into regions with different grid sizes. The grid size in coarse region is about $\left(\frac{1}{20} \sim \frac{1}{10}\lambda_{\max}\right)$ as in normal FDTD, while in the fine region the grid size is scaled by an integer ratio. As an example, the Yee cells with subgridding structure are shown in Figure 2, of which the scaling ratio is 1:3. For the time domain scattering and/or inverse scattering problem, the scatterers can be assigned with the fine region such that the fine structure can be easily described. If higher resolution is needed, only the fine region needs to be rescaled using a higher ratio for subgridding. This can avoid gridding the whole problem space using the finest resolution such that the computational resources are utilized in a more efficient way, which is quite important for the computational intensive inverse scattering problems.

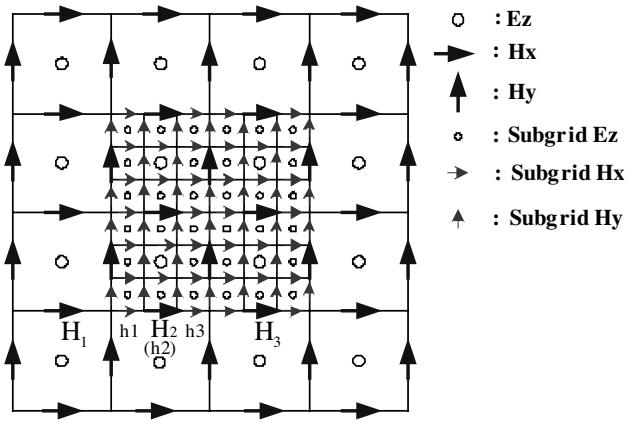

Figure 2. The structure of the TM_z FDTD major grids and local grids for the scaling ratio (1:3): H fields are aligned with the MG-LG boundary.

Because non-magnetic material is used in this study, the interfaces of the major grid and local grid (MG-LG) are set along with those lines containing the H fields as shown in Figure 2.

Since the permeability and thus the magnetic fields are continues across the MG-LG interfaces, no special treatment is required for evaluating the magnetic fields at those interfaces.

In Figure 2, E and H stand for the electric and magnetic fields on the major grids, respectively, while e and h denote the electric and magnetic fields on the local grids. If the scaling ratio is set at odd-ratio, for example $1:3$, then the E and H fields coincide with e and h fields in the fine region and in the time domain as shown in Figure 2 and Figure 3, respectively. Figure 3 shows the corresponding update sequence for the E, H, e and h fields in the fine region of Figure 2. Since the local grid size is one third of the main grid size, the time stepping interval $\Delta t'$ for the e and h fields on the local grids is also one third of that for the E and H fields on the main grids.

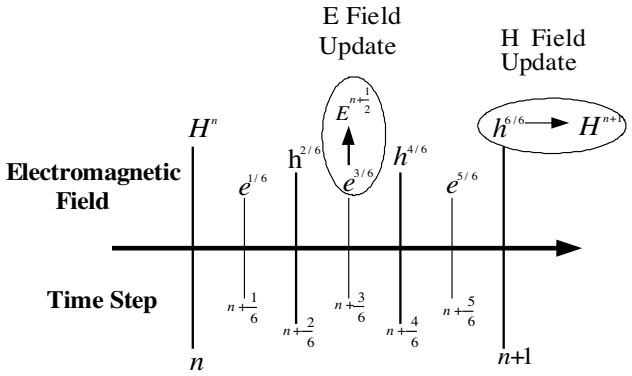

Figure 3. The update sequence for the (E, H) fields and (e, h) fields in the fine region of Figure 2.

Note that the e and h fields inside the fine region can be updated through the normal Yee-cell algorithm except those at the MG-LG boundary, such as h_1, h_2 and h_3 in Figure 2, for example.

The h fields at the MG-LG interface can be linearly interpolated as follows:

$$\begin{aligned} h_1^{n+v} &= H_1^{n+v} + 2/3\left(H_2^{n+v} - H_1^{n+v}\right) \\ h_2^{n+v} &= H_2^{n+v}, \qquad \text{for } \; v = \frac{1}{3},\ \frac{2}{3} \text{ and } \frac{3}{3} \\ h_3^{n+v} &= H_2^{n+v} + 1/3\left(H_3^{n+v} - H_2^{n+v}\right) \end{aligned} \tag{1}$$

Note that for (1) the H^{n+v} fields don't exist on the main grids actually for $v = \frac{1}{3}$ and $\frac{2}{3}$ and need extra parabolic interpolation calculation by

$$H^{n+v} = H^n + Av + \frac{Bv^2}{2} \tag{2}$$

with

$$A = \frac{H^{n+1} - H^{n-1}}{2}$$
$$B = H^{n+1} - H^{n-1} - 2H^n$$

The flow chart associated with Figure 3 to update the fields in the fine region is shown in Figure 4. Note that at the time step $n + \frac{3}{6}$ the $E^{n+\frac{1}{2}}$ fields on the main grids should be updated by the coincided $e^{n+\frac{3}{6}}$ fields on the local grids. Similarly, at the time step $n + \frac{6}{6}$ the H^{n+1} fields are updated by the coincided $h^{n+\frac{6}{6}}$ fields.

Finally, in order to avoid the unstability due to the mismatch of grid size at MG-LG interface, the h_2 fields right next to the H_1 fields of the MG-LG boundary as shown in Figure 5 are updated by

$$h_2 = \alpha h_2 + (1 - \alpha)\left(\frac{H_1 + h_3}{2}\right) \tag{3}$$

while the coincided E_2 and e_2 fields right closest to the MG-LG boundary are updated by

$$\begin{aligned} E_2 &= \beta E_2 + (1 - \beta)e_2 \\ e_2 &= (1 - \beta)E_2 + \beta e_2 \end{aligned} \tag{4}$$

where $\alpha = 0.95$ and $\beta = 0.8$ are adopted in this paper.

2.2. Inverse Problem

For the inverse scattering problem, the shape, location and permittivity of the dielectric cylinder are reconstructed by the given scattered electric field obtained at the receivers. This problem is resolved by an optimization approach, for which the global searching scheme PSO is employed to minimize the following cost function (CF):

$$CF = \frac{\sum_{n=1}^{N_i}\sum_{m=1}^{M}\sum_{t=0}^{T}\left|E_z^{\exp}(n,m,t) - E_z^{cal}(n,m,t)\right|}{\sum_{n=1}^{N_i}\sum_{m=1}^{M}\sum_{t=0}^{T}\left|E_z^{\exp}(n,m,t)\right|} \tag{5}$$

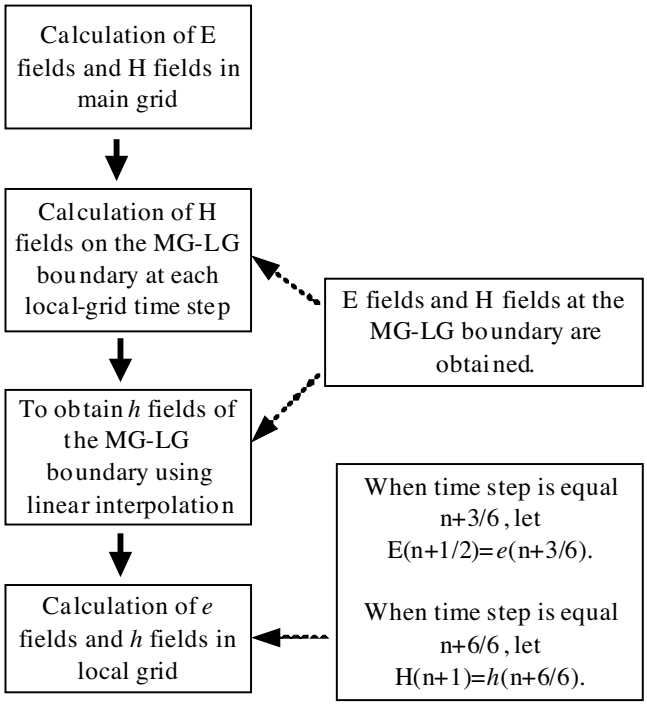

Figure 4. The flowchart to update the (E, H) fields on the major grids and (e, h) fields on local grids.

where $E_z^{\exp}$ and E_z^{cal} are experimental electric fields and the calculated electric fields, respectively. The N_i and M are the total number of the transmitters and receivers, respectively. T is the time duration of the recorded electric fields.

2.2.1. Particle Swarm Optimization (PSO)

Particle swarm optimization (PSO) was proposed by Kennedy and Eberhart in 1995 which is a population-based, self-adaptive search optimization technique. It is a kind of swarm intelligence that is based on social behavior. The social behavior in PSO is a population of particles moving towards the most promising region of the search space.

The PSO is initialized with a population of random solutions which assigns a randomized velocity to each potential solution, called the particle. Thus, each particle has a position and velocity vector, and moves through the problem space. In each generation, the particle changes its velocity by its best experience, called *pbest*, and that of the

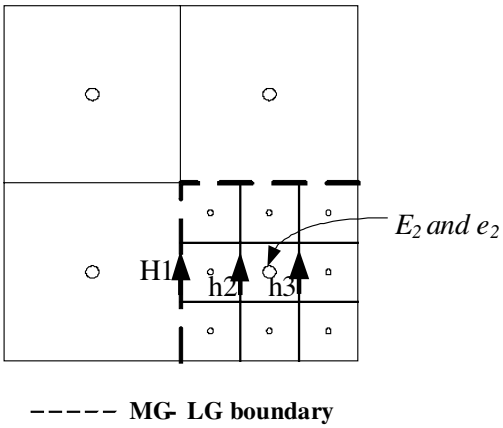

Figure 5. The relation of the E, H , e and h fields that used to enhance the stability.

best particle in the swarm, called *gbest*. Assume there are N_p particles in the swarm that is in a search space in D dimensions, the position and velocity could be determine according to the following equations:

$$v_{id}^{k} = w \cdot v_{id}^{k-1} + c_1 \cdot \varphi_1 \cdot \left(pbest_{id} - x_{id}^{k-1} \right) + c_2 \cdot \varphi_2 \cdot \left(gbest_d - x_{id}^{k-1} \right) \quad (6)$$

$$x_{id}^{k} = x_{id}^{k-1} + v_{id}^{k} \quad (7)$$

where v_{id}^{k} and x_{id}^{k} are the velocity and position of the i-th particle in the d-th dimension at k-th generation, φ_1 and φ_2 are both the random number between 0 and 1, c_1 and c_2 are learning coefficients and w is the inertial weighting factor that can avoid the particle trapped into the local minimized solution. After generations, the PSO can find the best solution according to the best solution experience.

2.2.2. Cubic Spline Interpolation Technique

In order to reduce the unknowns required to describe the arbitrary cylinder, the shape function of the cylinder is expressed in terms of a cubic spline. As shown in Figure 6, the cubic spline consists of the polynomials of degree 3 $P_i(\theta)$, $i = 1, 2, \ldots, N$, which satisfy the following smooth conditions:

$$\begin{aligned} P_i(\theta_i) &= P_{i+1}(\theta_i) = \rho_i \\ P_i'(\theta_i) &= P_{i+1}'(\theta_i) \qquad i = 1, 2, \ldots, N \\ P_i''(\theta_i) &= P_i''(\theta_i) \end{aligned} \quad (8)$$

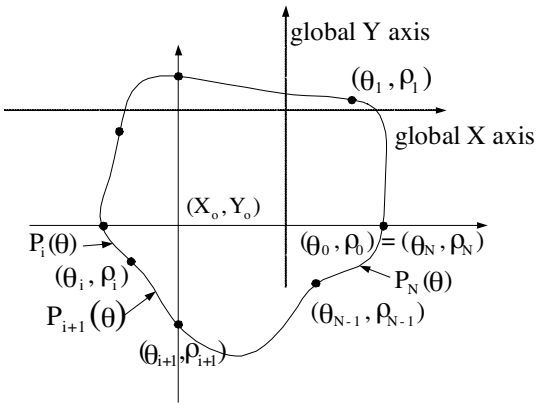

Figure 6. A cylinder of arbitrary shape is described in terms of the cubic spline.

and

$$\begin{aligned} P_1(\theta_0) &= P_N(\theta_N) \\ P_1'(\theta_0) &= P_N'(\theta_N) = \rho_N' \\ P_N''(\theta_i) &= P_N''(\theta_N) \end{aligned} \tag{9}$$

Through the interpolation of the cubic spline, an arbitrary smooth cylinder can be easily described through a few parameters ρ_1, ρ_2, ... , ρ_N and the slope ρ_N', the details are referred to [38]. By combining the PSO and the cubic spline interpolation technique, we are able to reconstruct the microwave image efficiently.

3. NUMERICAL RESULTS

As shown in Figure 1, the problem space is divided in 68×68 grids with the grid size $\Delta x = \Delta y = 1.47\,\text{cm}$. The homogeneous dielectric cylinder is located in free space. The cylindrical object is illuminated by a transmitter at four different positions, $N_i = 4$. The scattered E fields for each illumination are collected at the eight receivers, $M = 8$. The transmitters and receivers are collocated at a distance of 24 grids from the origin. The excitation waveform $I_z(t)$ of the transmitter is the Gaussian pulse, given by:

$$I_z(t) = \begin{cases} Ae^{-\alpha(t-\beta\Delta t)^2}, & t \le T_w \\ 0, & t > T_w \end{cases} \tag{10}$$

where $\beta = 24$, $A = 1000$, $\Delta t = 34.685\,\text{ps}$, $T_w = 2\beta\Delta t$, and $\alpha = \left(\frac{1}{4\beta\Delta t}\right)^2$.

The time duration T is set to $300\Delta t$. Note that in order to accurately describe the shape of the cylinder, the subgridding FDTD technique is used both in the forward scattering (1:9) and the inverse scattering (1:5) parts — but with different scaling ratios as indicated in the parentheses. For the forward scattering, the E fields generated by the FDTD with fine subgrids are used to mimic the experimental data in (5).

Three examples are investigated for the inverse scattering of the proposed structure by using the PSO. There are twelve unknown parameters to retrieve, which include the center position (X_0, Y_0), the radius ρ_i, $i = 1, 2, \ldots, 8$ of the shape function and the slope ρ'_N plus the relative permittivity of the object, $\varepsilon_r = \varepsilon_2/\varepsilon_0$. Very wide searching ranges are used for the PSO to optimize the const function given by (5). The parameters and the corresponding searching ranges are listed follow: $-30.88\,\text{cm} \le X_0 \le 30.88\,\text{cm}$, $-30.88\,\text{cm} \le Y_0 \le 30.88\,\text{cm}$, $0\,\text{cm} \le \rho_i \le 11.8\,\text{cm}$, $i = 1, 2, \ldots, 8$, $-1 \le \rho'_N \le 1$ and $1 \le \varepsilon_r \le 15$. The relative coefficient of the PSO are set as below: The learning coefficients, c_1 and c_2, are both set to 2. The inertial weighting factor is set to 0.4 and the population size set to 120.

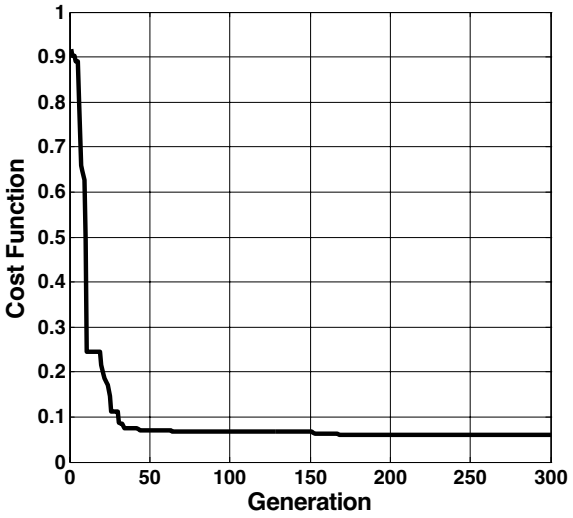

Figure 7. The average fitness value versus generation for example 1 using the Gaussian pulse illumination as the PSO executed five times.

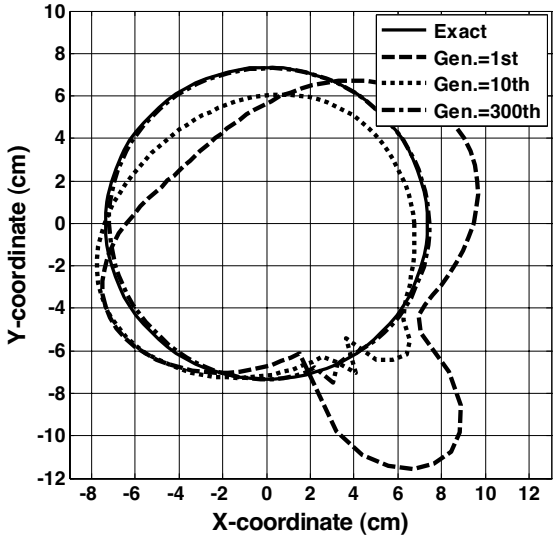

Figure 8. The reconstructed shape of the cylinder at different generations for example 1.

The first example, a simple circular cylinder is tested, of which the shape function $F(\theta)$ is chosen to be $F(\theta) = 7.352\,\text{cm}$, and the relative permittivity of the object is $\varepsilon_r = 3$. The average convergence curve of cost function versus generation as the PSO executed five times is shown in Figure 7. The reconstructed shape function of the best population member (particle) is plotted in Figure 8 for different generation. The final reconstructed shape and the cylinder position (X_0^c, Y_0^c) are compares to the exact shape and the position (X_0, Y_0) in Figure 9. It is observed that even reconstructed cylinder position (X_0^c, Y_0^c) is far away from exact one, the cubic spline interpolation technique can still recover it well. The r.m.s. error (DF) of the reconstructed shape $F^{cal}(\theta)$ and the relative error (DIPE) of ε_r^{cal} with respect to the exact values versus generation are shown in Figure 10. Here, DF and DIPE are defined as

$$DF = \left\{ \frac{1}{N'} \sum_{i=1}^{N'} \left[F^{cal}(\theta_i) - F(\theta_i) \right]^2 / F^2(\theta_i) \right\}^{1/2} \tag{11}$$

$$DIPE = \frac{\left| \varepsilon_r^{cal} - \varepsilon_r \right|}{\varepsilon_r} \tag{12}$$

where the N' is set to 160. The r.m.s. error DF is about 1.77% and DIPE= 0.97% in final. It is seen that the reconstruction is good.

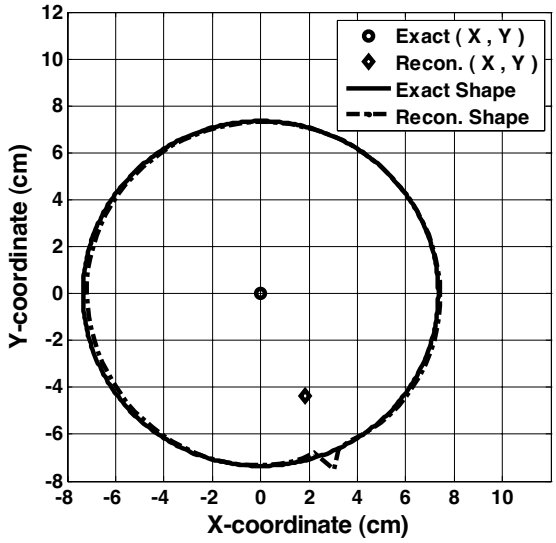

Figure 9. The final reconstructed shape and center position of the cylinder compared to the exact ones for example 1.

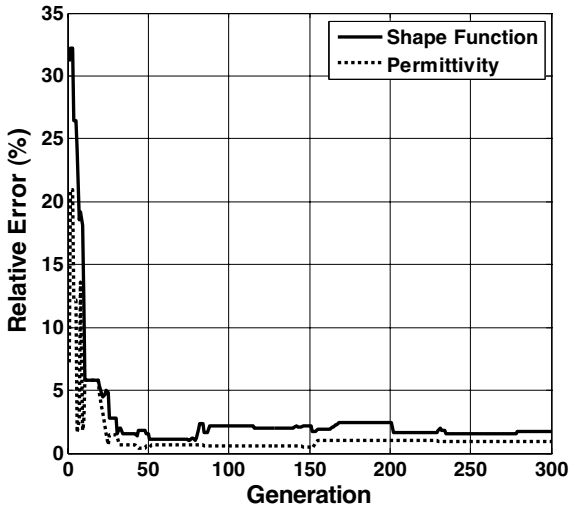

Figure 10. Shape-function error and permittivity error at each generation of example 1.

In the second example, the dielectric cylinder with shape function $F(\theta) = 5.88 - 1.47\sin(2\theta)$ cm and relative permittivity $\varepsilon_r = 3.5$ is considered. The reconstructed images for different generations and the relative error of this object are shown in Figure 11 and Figure 12, respectively. The r.m.s. error DF is about 4.8% and DIPE=1.8% in final generation. From the reconstructed result of this object, we conclude the proposed method can be used to reconstruct dielectric cylinder successfully when the dielectric object with high-contrast permittivity.

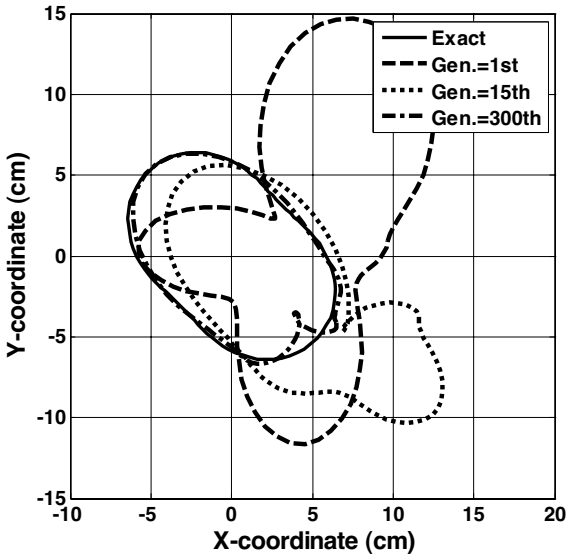

Figure 11. The reconstructed cross section of the cylinder of example 2 at sequential generations.

The reconstructed result of the final example is shown in Figure 13, where the shape is $F(\theta) = 5.88 + 1.47\cos(\theta) + 2.94\cos(3\theta)$ cm, and the relative permittivity of the object is $\varepsilon_r = 3.2$. Figure 14 shows that the relative errors of the shape and the permittivity decrease quickly by generations. The r.m.s. error DF is about 4.45% and DIPE = 1.5%. In order to investigate the sensitivity of the imaging algorithm against random noise, the additive white Gaussian noise of zero mean is added into the experimental electric fields. The signal to noise ratio (SNR)

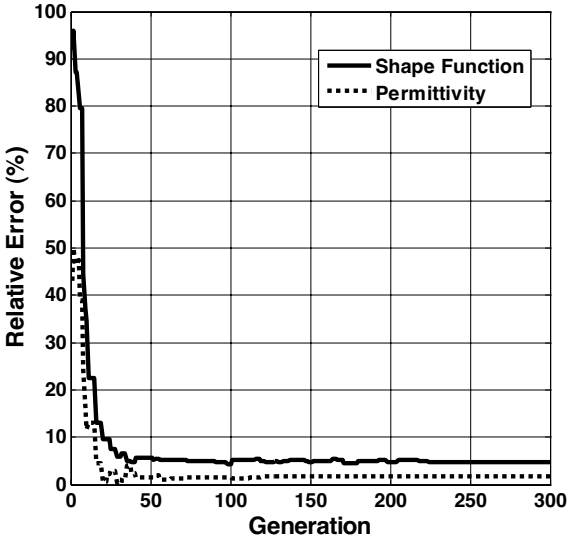

Figure 12. Shape-function error and permittivity error at different generations of example 2.

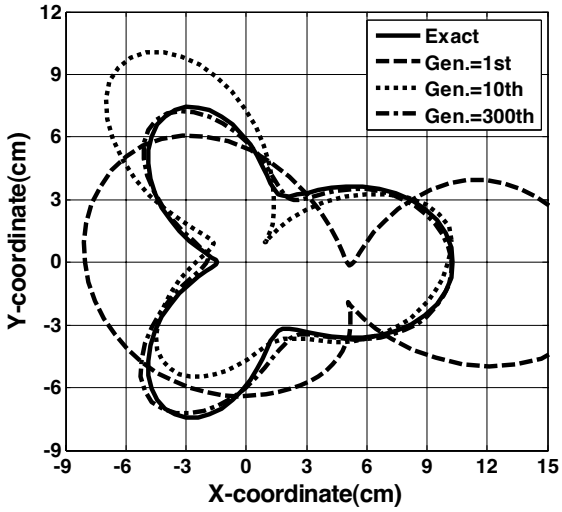

Figure 13. The reconstructed cross section of the cylinder of example 3 at sequential generations.

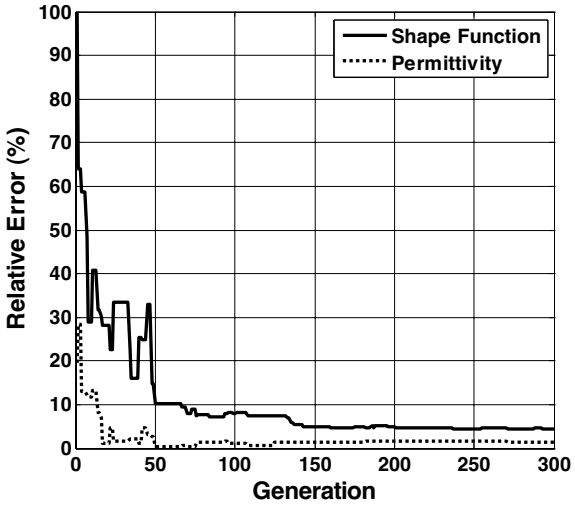

Figure 14. Shape-function error and permittivity error at different generations of example 3.

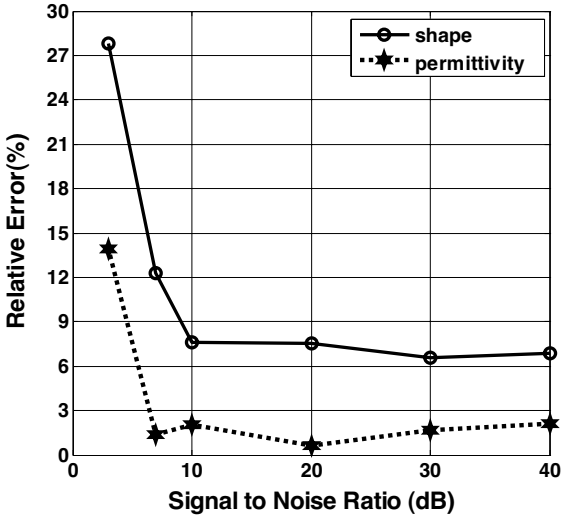

Figure 15. Shape error and the relative permittivity errors as functions of SNR (dB).

is define as:

$$SNR = 20\log_{10}\frac{\sum_{n=1}^{Ni}\sum_{m=1}^{M}\sum_{t=0}^{T}|E_z^{\exp}(n,m,t)|}{\sum_{n=1}^{Ni}\sum_{m=1}^{M}\sum_{t=0}^{T}|noise(n,m,t)|} \tag{13}$$

Figure 15 shows the reconstructed results under the condition that the experimental scattered field is contaminated by noise. The SNR include 40 dB, 30 dB, 20 dB, 10 dB, 7 dB and 3 dB for simulation purpose. It could be observed that good reconstruction has been obtained for both the relative permittivity and shape of the dielectric cylinder when the SNR is above 10 dB.

4. CONCLUSION

We present a study of the time domain inverse scattering of an arbitrary cross section dielectric cylinder in free space. By combining the FDTD method and the PSO, good reconstructed results are obtained by using Gaussian pulse illuminations. The subgridding scheme is employed to closely describe the shape of the cylinder for the FDTD method. Some stabilization techniques to avoid the mismatch at the MG-LG interface are adopted. The forward problem is solved by using the subgridding FDTD method and the shape function of the cylinder is approximated by Fourier series expansion. The inverse problem is reformulated into an optimization one, and then the global searching scheme PSO is employed to search the parameter space. Interpolation technique through cubic spline is utilized to reduce the number of parameters needed to describe an arbitrary shape. By using the PSO, the shape, location and dielectric constant of the object can be successfully reconstructed even when the dielectric constant is fairly large. In our study, even when the initial guess is far from the exact one, the PSO can still yield a good solution for the properties of the object, while the gradient-based methods often get stuck in a local extreme. Numerical results have been carried out and good reconstruction has been obtained even in the presence of white Gaussian noise in experimental data.

REFERENCES

1. Yapar, A., H. Şahintürk, I. Akduman, and R. Kress, "One-dimensional profile inversion of a cylindrical layer with inhomogeneous impedance boundary: A Newton-type iterative solution," *IEEE Transactions on Geoscience and Remote Sensing*, Vol. 43, No. 10, 2192–2199, Oct. 2005.
2. Ma, J., W. C. Chew, C. C. Lu, and J. Song, "Image reconstruction from TE scattering data using equation of strong permittivity fluctuation," *IEEE Transactions on Antennas and Propagation*, Vol. 48, No. 6, 860–867, June 2000.
3. Otto, G. P. and W. C. Chew, "Microwave inverse scattering-local shape function imaging for improved resolution of strong scatterers," *IEEE Transactions on Microwave Theory and Techniques*, Vol. 42, No. 1, 137–142, Jan. 1994.
4. Chiu, C. C. and Y. W. Kiang, "Microwave imaging of multiple conducting cylinders," *IEEE Transactions on Antennas and Propagation*, Vol. 40, No. 8, 933–941, August 1992.
5. Chien, W. and C. C. Chiu, "Using NU-SSGA to reduce the searching time in inverse problem of a buried metallic object," *IEEE Transactions on Antennas and Propagation*, Vol. 53, No. 10, 3128–3134, Oct. 2005.
6. Qing, A., "An experimental study on electromagnetic inverse scattering of a perfectly conducting cylinder by using the real-coded genetic algorithm," *Microwave and Optical Technology Letters*, Vol. 30, 315–320, Sept. 2001.
7. Caorsi, S., A. Massa, and M. Pastorino, "A computational technique based on a real-coded genetic algorithm for microwave imaging purposes," *IEEE Transactions on Geoscience and Remote Sensing*, Vol. 38, No. 4, 1697–1708, July 2000.
8. Takenaka, T., Z. Q. Meng, T. Tanaka, and W. C. Chew, "Local shape function combined with genetic algorithm applied to inverse scattering for strips," *Microwave and Optical Technology Letters*, Vol. 16, 337–341, Dec. 1997.
9. Wei, C., "Inverse scattering of an un-uniform conductivity scatterer buried in a three-layer structure," *Progress In Electromagnetics Research*, PIER 82, 1–18, 2008.
10. Huang, C.-H., Y.-F. Chen, and C.-C. Chiu, "Permittivity distribution reconstruction of dielectric objects by a cascaded method," *Journal of Electromagnetic Waves & Applications*, Vol. 21, No. 2, 145–159, 2007
11. Thomas, V., C. Gopakumar, J. Yohannan, A. Lonappan,

G. Bindu, A. V. P. Kumar, V. Hamsakutty, and K. T. Mathew, "A novel technique for localizing the scatterer in inverse profiling of two dimensional circularly symmetric dielectric scatterers using degree of symmetry and neural networks," *Journal of Electromagnetic Waves & Applications*, Vol. 19 No. 15, 2113–2121, 2005.

12. Yagle, A. E. and J. L. Frolik, "On the feasibility of impulse reflection response data for the two-dimensional inverse scattering problem," *IEEE Transactions on Antennas and Propagation*, Vol. 44, No. 12, 1551–1564, Dec. 1996.
13. Yu, W., Z. Peng, and L. Jen, "The time-domain born iterative method for two-dimensional inhomogeneous lossy dielectric," *Journal of Microwaves*, Vol. 11, No. 12, 1995.
14. Chaturvedi, P. and R. G. Plumb, "Electromagnetic imaging of underground targets using constrained optimization," *IEEE Transactions on Geoscience and Remote Sensing*, Vol. 33, No. 3, 551–561, May 1995.
15. Moghaddam, M. and W. C. Chew, "Study of some practical issues in inversion with the Born iterative method using time-domain data," *IEEE Transactions on Antennas and Propagation*, Vol. 41, No. 2, 177–184, Feb. 1993.
16. Weedon, W. H., "Broadband microwave inverse scattering: Theory and experiment," Ph.D. dissertation, University of Illinois at Urbana-Champaign, 1994.
17. Weedon, W. H. and W. C. Chew, "Time-domain inverse scattering using the local shape function (LSF) method," *Inverse Problem*, Vol. 9, 551–64, Oct. 1993.
18. Rekanos, I. T., "Time-domain inverse scattering using lagrange multipliers: An iterative FDTD-based optimization technique," *Journal of Electromagnetic Waves and Applications*, Vol. 17, No. 2, 271–289, 2003.
19. Kang, N. W., Y. S. Chung, C. Cheon, and H. K. Jung, "A new 2-D image reconstruction algorithm based on FDTD and design sensitivity analysis," *IEEE Transactions on Microwave Theory and Techniques*, Vol. 50, No. 12, 2734–2740, Dec. 2002.
20. Takenaka, T., H. Jia, and T. Tanaka, "Microwave imaging of electrical property distributions by a forward-backward time-stepping method," *Journal of Electromagnetic Waves Application*, Vol. 14, 1609–1625, 2000.
21. He, S., P. Fuks, and G. W. Larson, "An optimization approach to time-domain electromagnetic inverse problem for a stratified dispersive and dissipative slab," *IEEE Transactions on Antennas*

and Propagation, Vol. 44, No. 9, 1277–1282. Sept. 1996.

22. Zhong, X.-M., C. Liao, and W. Chen, "Image reconstruction of arbitrary cross section conducting cylinder using UWB pulse," *Journal of Electromagnetic Waves Application*, Vol. 21, No. 1, 25–34, 2007.
23. Chen, X., D. Liang, and K. Huang, "Microwave imaging 3-D buried objects using parallel genetic algorithm combined with FDTD technique," *Journal of Electromagnetic Waves Application*, Vol. 20, No. 13, 1761–1774, 2006.
24. Huang, C. H., S. H. Chen, C. L. Li, and C. C. Chiu, "Time domain inverse scattering of an embedded cylinder with arbitrary shape using nearly resonant technique," *2004 International Conference on Electromagnetic Applications and Compatibility*, Taipei, Taiwan, Oct. 2004.
25. Bermani, E., S. Caorsi, and M. Raffetto, "Geometric and dielectric characterization of buried cylinders by using simple time-domain electromagnetic data and neural networks," *Microwave and Optical Technology Letters*, Vol. 24, No. 1, 24–31, Jan. 2000.
26. Isakov, V., "Uniqueness and stability in multidimensional inverse problems," *Inverse Problems*, Vol. 9, No. 6, 579–621, 1993.
27. Kirsch, A. and R. Kress, "Uniqueness in inverse obstacle scattering," *Inverse Problems*, Vol. 9, 285–299, 1993.
28. Colton, D. and L. Paivarinta, "The uniqueness of a solution to an inverse scattering problem for electromagnetic waves," *Archive for Rational Mechanics and Analysis*, Vol. 119, No. 1, 59–70, March 1992.
29. Colton, D. and R. Kress, *Inverse Acoustic and Electromagnetic Scattering Theory*, Springer-Verlag, New York, 1992.
30. Eberhart, R. C. and J. Kennedy, "A new optimizer using particle swarm theory," *Proceedings of the Sixth International Symposium on Micro Machine and Human Science*, 39–43, Japan, 1995.
31. Donelli, M. and A. Massa, "Computational approach based on a particle swarm optimizer for microwave imaging of two-dimensional dielectric scatterers," *IEEE Transactions on Microwave Theory and Techniques*, Vol. 53, No. 5, 1761–1776, May 2005.
32. Semnani, A. and M. Kamyab, "An enhanced method for inverse scattering problems using fourier series expansion in conjunction with FDTD and PSO," *Progress In Electromagnetics Research*, PIER 76, 45–64, 2007.
33. Caorsi, S., M. Donelli, A. Lommi, and A. Massa, "Location and

imaging of two-dimensional scatterers by using a particle swarm algorithm," *Journal of Electromagnetic Waves & Applications*, Vol. 18, No. 4, 481–494, 2004.

34. Huang, T. and A. S. Mohan, "Application of particle swarm optimization for microwave imaging of lossy dielectric objects," *2005 IEEE Antenna and Propagation Society International Symposium Digest*, 852–855, 2005.
35. Semnani and M. Kamyab, "Truncated cosine fourier series expansion method for solving 2-d inverse scattering problems," *Progress In Electromagnetics Research*, PIER 81, 73–97, 2008.
36. Taflove, A. and S. Hagness, *Computational Electrodynamics: The Finite-Difference Time-Domain Method*, Artech House, Boston, MA, 2000.
37. Chevalier, M. W., R. J. Luebbers, and V. P. Cable, "FDTD local grid with materical traverse," *IEEE Trans. Antennas and Propagation*, Vol. 45, No. 3, March 1997.
38. De Boor, C., *A Practical Guide to Splines*, Springer-Verlag, New York, 1978.
39. Li, C.-L., C.-W. Liu, and S.-H. Chen, "Optimization of a PML absorber's conductivity profile using FDTD," *Microwave and Optical Technology Letters*, Vol. 37, No. 5, 69–73, Jun. 2003.
40. Yee, K., "Numerical solution of initial boundary value problems involving Maxwell's equations in isotropic media," *IEEE Transactions on Antennas and Propagation*, Vol. 14, No. 3, 302–307, May 1966.